Environmental Modelling & Software 95 (2017) 13–21

Contents lists available at ScienceDirect

Environmental Modelling & Software

journal homepage: www.elsevier.com/locate/envsoft

Terrestrial laser scanning improves digital elevation models and topsoil pH modelling in regions with complex topography and dense vegetation

Andri Baltensweiler [a, *], Lorenz Walthert [a], Christian Ginzler [a], Flurin Sutter [a], Ross S. Purves [b], Marc Hanewinkel [c]

[a] Swiss Federal Institute for Forest, Snow and Landscape Research WSL, Birmensdorf, Switzerland
[b] Department of Geography, University of Zurich, Zurich, Switzerland
[c] Chair of Forestry Economics and Forest Planning, University of Freiburg, Freiburg, Germany

ARTICLE INFO

Article history:
Received 7 October 2016
Received in revised form
26 February 2017
Accepted 24 May 2017

Keywords:
Digital elevation model
Terrestrial laser scanning
Airborne LiDAR
Accuracy
Digital soil mapping
Terrain attribute

ABSTRACT

Terrestrial Laser Scanning (TLS) has great potential in creating high resolution digital elevation models (DEMs). However, little is known about the properties of TLS derived DEMs covering several hectares in heterogeneous environments compared to conventional airborne laser scanning (ALS) based models and their influence on derived products. We investigated the accuracy of DEMs with different resolutions derived from TLS and high quality ALS on a study site with complex micro-topography covered by dense forest and ground vegetation. We further examined the effect of these DEMs on predicted topsoil pH using linear regression models built on terrain attributes. We show that at high resolutions (~1 m), TLS based DEMs performed better than ALS DEMs, which directly translated into significantly better pH models, the best of which showing an R^2 of 0.62. The use of TLS therefore improves the quality of terrain attributes, which are the foundation for many ecological and hydrological applications.

1. Introduction

Digital elevation models (DEMs) are indispensable tools in describing many landsurface forms and processes. They are used in many different fields including hydrological modelling (e.g. Gurtz et al., 1999; Yang et al., 2014) geomorphological (Lin et al., 2013) and digital soil mapping (e.g. McBratney et al., 2003; Nussbaum et al., 2014), natural hazard assessment (e.g. Arnone et al., 2016; Bühler et al., 2015), or ecological species distribution models (e.g. Camathias et al., 2013; Guisan and Zimmermann, 2000). A very widely used source of DEM data is light detection and ranging (LiDAR), a technology which permits creation of high resolution and accurate DEMs (Tarolli, 2014). LiDAR measures the distance between a sensor and a target based on half the elapsed time between the emission of a pulse and the detection of a reflected return (Baltsavias, 1999). Most DEMs derived from LiDAR rely on airborne laser scanning (ALS). ALS surveys are typically designed to have a dense and evenly distributed LiDAR point density over large areas (Bater and Coops, 2009). The accuracy of DEMs generated by ALS is dependent on a range of factors including flight altitude above ground level, flight speed and scan angle (Hyyppä et al., 2008; Maguya et al., 2014). Dense vegetation cover such as multi-story forests and dense ground vegetation can reduce the penetration rate of the LiDAR pulses to the ground (Guan et al., 2014; Hodgson et al., 2003; Mulder et al., 2011) and thus also influence DEM accuracy. To derive a DEM, LiDAR reflection points need to be separated into non-ground points, e.g. vegetation returns, and ground points. This can be especially challenging in regions with complex topography and dense vegetation cover, which is often the case in mountainous landscapes (Guan et al., 2014; Maguya et al., 2014; Montealegre et al., 2015). Moreover, several studies have shown that DEM error increases as the ground point density decreases (Anderson et al., 2006; Chu et al., 2014; Jakubowski et al., 2013).

The vertical accuracy of ALS based DEMs in forested and mountainous regions has been assessed in various publications (Bater and Coops, 2009; Kobler et al., 2007; Montealegre et al., 2015). Root Mean Square Errors (RMSEs) of models between 0.16

* Corresponding author.
E-mail address: andri.baltensweiler@wsl.ch (A. Baltensweiler).

http://dx.doi.org/10.1016/j.envsoft.2017.05.009

and 0.37 m were reported with a point density ranging from 0.7 to 8.5 points/m^2. Bater and Coops (2009) showed that the resolution of DEMs, generated from the same LiDAR ground points, influence DEM accuracy, independently of the applied interpolation method. They created DEMs at spatial resolutions of 0.5, 1.0 and 1.5 m and obtained RMSEs of 0.17, 0.19 and 0.25 m. However, these error values were strongly influenced by the spatial scale of the terrain variation. Cell resolution selection should be based on point density and distribution, horizontal accuracy, terrain complexity (Hengl, 2006) and on the relevant scale for the process or attribute being modeled (Cavazzi et al., 2013; Fisher et al., 2004; Liu, 2008).

The application of terrestrial laser scanning (TLS) has rapidly increased in recent years for purposes including topographical surveys (Gallay et al., 2013), investigations of small scale landslides (Wang et al., 2013) or collecting forest inventory measurements (Dassot et al., 2011; Marselis et al., 2016; Moskal and Zheng, 2011). TLS enables fast and dense height sampling from the surface of objects in the neighborhood of the scanner. The accuracy of these point measurements is in the range of that obtained by a total station. Heritage et al. (2009) reported a median error of −0.003 m for 186 surface points, measured with a total station and a terrestrial laser scanner. TLS is limited to substantially smaller areas than ALS because of the low oblique angle of transmitted signals. In addition, LiDAR impulses can be reflected back to the scanner by obstacles and therefore shadows occur in the 3D point cloud. This is mainly an issue in dense forests with understory and/or areas with a rugged topography (Panholzer and Prokop, 2013). In contrast to ALS which acquires the data at near nadir view angles and thereby yield a relatively homogenous point distribution, TLS generates an irregular distribution of points. The TLS points concentrate around the scanner and density decreases inversely proportional to the square of the distance to the scanner location (Hilker et al., 2010). To mitigate these effects and to generate a 3D point cloud with a larger spatial extent, multiple TLS scans with different viewsheds can be combined in a single dataset. To scan e.g. an area of 60 m^2 in a pine forest for tree canopy studies, 3 scans were required (Danson et al., 2006), whereas 14 scans were taken to survey 36′000 m^2 in a glacial valley to monitor cliff evolution (Heritage and Hetherington, 2007). Due to the irregular point distribution and the shadowing effect of obstacles the separation of ground and non-ground points obtained by TLS is more complex than for ALS data (Panholzer and Prokop, 2013; Rodríguez-Caballero et al., 2016).

So far, relatively few studies have discussed the accuracy of DEMs derived from TLS data and the resulting influence on derived terrain properties. Typically, RMSEs vary considerably depending on the site characteristics. Gallay et al. (2013) compared the accuracy of DEMs derived from TLS data and ALS last return echoes. For a flat terrain with low-cut meadow, the reported RMSEs were 0.007 m for TLS and 0.286 m for ALS data. In an uneven slope covered by dense vegetation the corresponding RMSE were 0.525 m and 0.306 m. However, no filter was applied to separate the point clouds. Pirotti et al. (2013) reported a RMSE of 0.3 m based on DEM composed of 7 scans with a resolution of 0.1 m. The study was conducted in a steep landslide area covered with pioneer species, coppice and tall trees.

For many ecological and environmental models, the spatial distribution of soil properties is a crucial input. To improve e.g. plant species distribution models, accurate and high resolution soil information are considered as a primary requirement (Guisan and Zimmermann, 2000) since the success of a species is largely conditioned by soil chemical properties (Walthert et al., 2013). However, spatially explicit soil data of sufficient quality is scarce, due to the complexity of soil geography and the hidden nature of soil. An added problem are the high costs for soil sampling and for most soil analyses (Rossiter, 2005). In recent years, the spatial availability of soil data has been increased through digital soil mapping (DSM) which has been proven to provide useful soil properties maps (e.g. Samuel-Rosa et al., 2015; Shary and Pinskii, 2013).

Terrain attributes (TAs) such as slope, curvature or topographic wetness index (TWI) act as soil forming factors and thus are related to soil forming processes. They can be derived from DEMs and are often used in DSM as key factors for inferring chemical and physical soil properties (McBratney et al., 2003). Slope and curvature determine the intensity and direction of flows of matter and therefore are relevant for erosion, leaching and accumulation processes (MacMillan and Shary, 2009; Shary and Pinskii, 2013; Wilson, 2012). Similarly, TWI combines upslope contributing area and local slope and is a proxy for soil moisture patterns (Moore et al., 1991; Seibert et al., 2007). The spatial scale of soil forming processes can vary from the very local up to landscape scales, as manifested in the spatial pattern and range of soil properties across a landscape. Therefore, the scale at which these processes operate should determine the optimal scale for deriving TAs (Fisher et al., 2004; Maynard and Johnson, 2014).

The scale-dependency of TAs to spatially predict soil properties suggests that there is an optimal scale to derive TAs for inferring soil properties (e.g. Cavazzi et al., 2013; Kim and Zheng, 2011; Maynard and Johnson, 2014; Pain, 2005; Park et al., 2009; Smith et al., 2006). For topography such as hillslopes, rolling hills, drumlins or dunes, moderate TAs resolutions (15–50 m) produced highest prediction accuracy whereas coarse scaled TAs (>100 m) were most suitable for flat areas. Various recent studies have emphasized that fine-scaled DEMs (resolution < 10 m) are not always the best choice for DSM studies (Cavazzi et al., 2013; Kim and Zheng, 2011; Maynard and Johnson, 2014). Kim and Zheng (2011) argued that soil contains a spatially diffusive nature from one location or grid cell to adjacent locations or cells and therefore edaphic traits (e.g. soil pH, nutrient content) can be influenced by lateral water flow. In a uniform substrate, e.g. sandy dunes, with highly homogenous edaphic conditions the capture of any mirco-scale topographic relief is therefore not desirable. In such uniform substrates, fine-resolution TAs might introduce high-frequency noise and do not typically improve spatial predictions (Cavazzi et al., 2013; Kim et al., 2011; Smith et al., 2006). In more rugged areas with a complex substrate structure, by contrast, the fine-resolution TAs are expected to be most suitable for DSM (Kim et al., 2011), who also emphasized that empirical research is needed to test this hypothesis.

To find the appropriate cell size and relevant scale for the process being modeled, a multiscale approach was introduced by Behrens et al. (2010) and Grinand et al. (2008) that incorporates different spatial scales in soil property prediction models. TAs derived from a DEM are smoothed by local average filters with distinct neighborhood sizes to integrate information of the neighborhood into the processed pixel whereas small scale variation is omitted (Liu et al., 2009). Although the scale-dependency of TAs in DSM has been discussed in many publications, the accuracy of different input DEMs in deriving TAs has not been investigated with respect to accuracy of soil properties modelling.

The first aim of this study was to investigate if DEMs derived from TLS data obtained from forested regions with dense vegetation achieve higher accuracies than DEMs based on high quality ALS data. Furthermore, the effect of different resolutions (0.2–4 m) and interpolation methods was addressed and compared with corresponding DEMs derived from ALS data. Secondly, we aimed to evaluate how accuracies and resolutions of DEMs obtained from ALS and TLS data affect the performance of topsoil pH models. For this, we performed a case study in a mountainous, forested site of 2 ha with a strong micro-topography. We derived a set of TAs for

diverse DEM resolutions and established ordinary least square regression (OLS) models.

2. Material and methods

2.1. Study site

The 2 ha study site is part of the Swiss Long-term Forest Ecosystem Research program LWF (Schaub et al., 2011) and located in the valley of Alptal in Switzerland (Fig. 1). It is a mountainous landscape at 1150 m above sea level. The climate is cool and wet (6 °C mean temperature and 2300 mm mean precipitation per year). Mean slope is about 20° and a strong micro-relief exists with ridges and depressions. The geological formation is Flysch, a tertiary sediment with alternating shists of calcareous sandstones, argillite and bentonite. The soils of the research site are classified as umbric Gleysoils (Schleppi et al., 1998). The main tree species is Norway spruce (Picea abies) with tree heights up to 33 m and a stand density of 1228 trees/ha. The ground vegetation consists mainly of blueberries (Vaccinium myrtillus) and different herbaceous species including wood horsetail (Equisetum sylvaticum), rusty sedge (Carex ferruginea), reed grass (Calamagrostis varia) and various mosses.

2.2. Data acquisition

ALS data were collected using a Riegl VZ-1000 mounted on an Ecureuil AS 350 B3 helicopter. Flight altitude and speed were 500 m above ground and 30 knots respectively. The average pulse density was 16.9 pulses/m^2. Because of dense vegetation, the full wave LiDAR system often recorded multiple returns resulting in an average echo density of 21.2 points/m^2. The size of the footprint was 0.15 m and the height accuracy was within 0.08 m (one standard deviation). The flight took place on 5th May 2015 after snowmelt to ensure that vegetation was minimally developed. Table 1 shows the

Table 1
Specification of the used scanners.

	Riegl VZ-1000	Faro Focus 3D S120
Range finder	Pulsed time-of-flight	Phase shift
Wavelength [nm]	Near-infrared	905 (Near-infrared)
Return type	Full wave	Single signal
Measurement range [m]	2.5–1200	0.6–120
Range accuracy [mm]	8 (at 100 m)	2 (at 25 m)
Beam diameter at exit [mm]	8	3
Beam divergence [mrad]	0.3	0.19
V x H field of view [°]	100 × 360	300 × 360
Acquisition rate (pts/s)	up to 122 000	up to 976 000
Weight incl peripherals [kg]	12	5

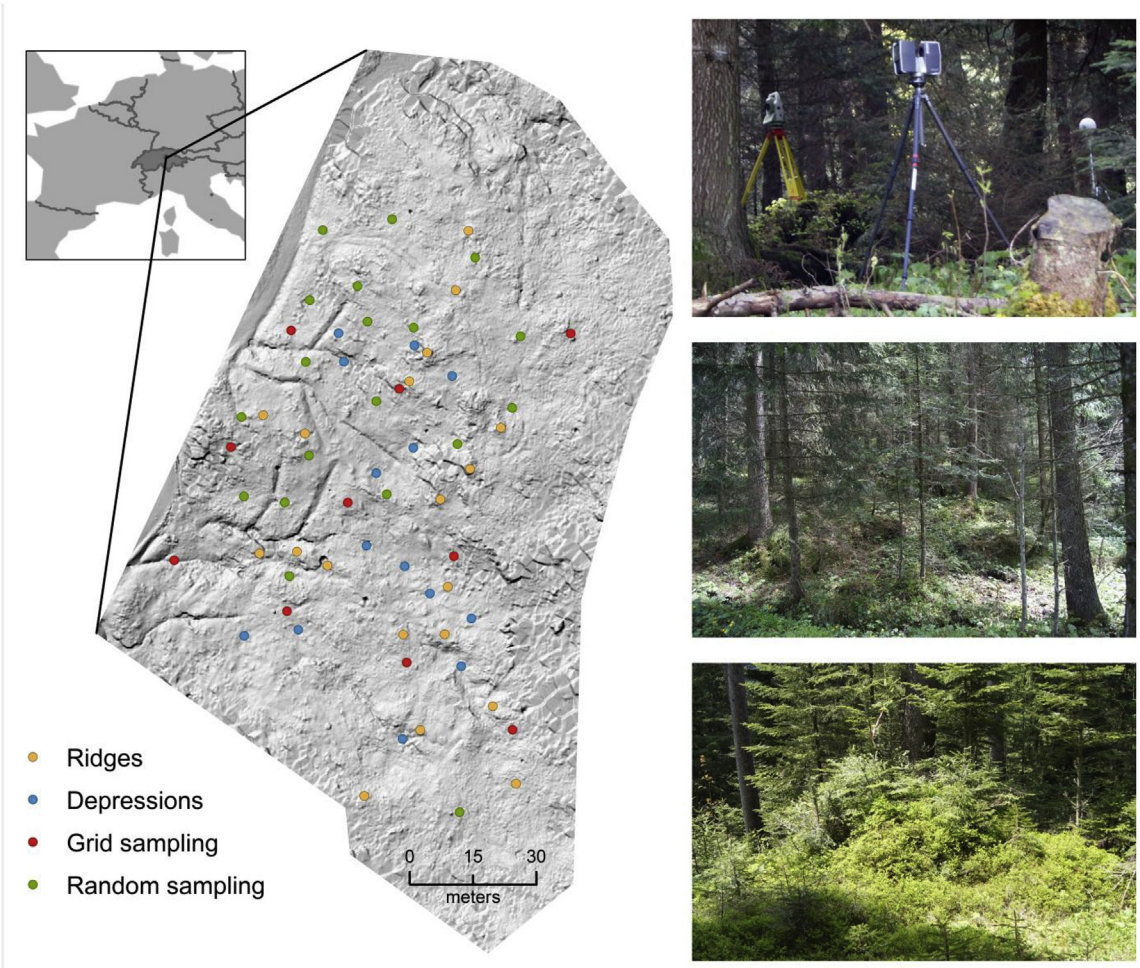

Fig. 1. Study site, Terrestrial Laser Scanning (TLS) assessment and soil sampling. Left: Location of the study site with shaded relief derived from TLS data (resolution 0.2 m) with locations of the soil samples. Upper right: TLS Faro Scanner, spherical reference target and Leica total station. Middle right: mirco-relief under dense conifer forest. Lower right: dense ground vegetation with young Norway spruces and blueberries.

specification of the laser scanner. This dataset is henceforth referred to as ALS data.

For the TLS data acquisition, a Faro Focus 3D 120 laser scanner was used (Table 1). The chosen point spacing was 6 mm at 10 m distance from the scanner. In order to scan the whole research area and to mitigate occlusions, 78 scans at different locations were carried out. The TLS point clouds were co-registered with separate highly reflective spherical reference targets as tie points to establish a relative orientation between the individual scans (Fig. 1). The targets were placed in the scan areas so that at least 3 common targets were visible in two neighboring scans. With the Faro Scene 5.2 software the targets were identified manually to coregister the individual scans (accuracy ± 5 mm). The targets were surveyed in the field using a Leica TCPR 1202 total station with an accuracy of ±2 mm. After the relative coregistration of the 78 scans they were transformed from the local coordinate system to the Swiss national coordinate system (CH1903LV03/LN02). It took about 5 working days to acquire TLS data in the field. The TLS field campaign was carried out between the end of May and the beginning of June 2013 at the same vegetation developmental stage as for ALS data. Because of more persistent snow cover, the vegetation development was delayed compared to 2015.

As a third LiDAR dataset the nationally available dataset SwissAlti provided by the Swiss Federal Office of Topography was used (Swisstopo, 2010). This dataset consists of discrete first and last LiDAR returns with a nominal footprint size of 0.3 m. The nominal point density in the study area was 0.69 points/m^2 and the reported standard deviation of height accuracy was 0.5 m in open areas and 1.5 m in forested areas (Artuso et al., 2003). The national data were acquired during multiple seasons between 2000 and 2007. For the study region the data were acquired in 2002.

2.3. Soil data

A total of 62 soil samples were taken in May and June 2013 whereby 56 sampling points were surveyed with Leica TCPR 1202 total station and 6 samples with Leica Disto D5 pointfinder. For the latter, no height values were recorded. In order to obtain an unbiased set of soil samples, the sample scheme was carefully designed. To represent the whole pH variation of the study site in the soil samples, a priori information about the pedogenetic process was used to stratify the area in ridges and depressions. Soils on ridges are characterized by a low pH as a result of intense weathering whereas an alkaline regime is characteristic in depressions due to a steady supply of basic cations (e.g. Ca and Mg) in the soil water solution. 19 points were sampled on ridges, 14 in depressions (Fig. 1). To cover the whole spatial extent, another 10 sampling points were placed on a regular grid. Additionally, 19 points were randomly sampled by applying the Random Points Function of ArcGIS (v.10.3, ESRI) to ensure that any location within the study area has an equal chance of being selected as a sampling point. At each sampling point, soil samples were taken at depths of 5–10 cm and 20–30 cm. The pH of each sample was measured in a 0.01 M $CaCl_2$ suspension in duplicate. To model the topsoil pH, only the pH values for the depth of 5–10 cm were used. The pH for this sample depth ranged between 3.5 and 7.0, with a mean of 5.14.

2.4. Point cloud processing

All LiDAR point clouds were processed with the software package of LAStools (Isenburg, 2015). In order to make the TLS point cloud operable for further data processing and to reduce point noise (Puttonen et al., 2015), data density was reduced by applying the lasthin function. A grid of 0.05 × 0.05 m was placed over the TLS points and within each cell only the point with the lowest height value was kept in the point cloud since our goal was to derive terrain. To separate LiDAR data into vegetation points and ground points, the lasground function was applied for all three LiDAR datasets with no manual editing. The lasground function is based on adaptive densification of a triangular irregular network (TIN) developed by Axelsson (2000). The initial sparse TIN is created from local minimum points over a defined area. To each triangle, new points are added depending on their positions and the geometry of the new triangles generated. This filter was originally developed for airborne LiDAR data and is also implemented in the common used LiDAR processing software TerraScan from TerraSolid.

2.5. DEM interpolation

In order to consider the influence of different resolutions and interpolation methods regarding to the final DEM accuracy, we applied the Inverse Distance Weighted (IDW) and the TIN method. Both methods are commonly used to generate DEMs from ALS (Chaplot et al., 2006; Guo et al., 2010; Sačkov and Kardoš, 2014) and TLS (Heritage et al., 2009; Lei and Atkinson, 2015) and are considered to perform well. In this study, IDW interpolation implemented in ArcGIS (v.10.3, ESRI) was used with a power of two and a variable search radius of the 12 nearest points. The TIN algorithm with linear interpolation and constrained Delaunay triangulation was performed with the function las2dem from the LAStools (Isenburg, 2015). Only classified ground points were used for the interpolations. For both interpolators and for the ALS and TLS dataset, DEMs were generated with spatial resolutions of 0.2, 0.5, 1, 2 and 4 m. For the LiDAR point cloud SwissAlti only DEMs with a spatial resolution of 2 m were generated using both interpolation methods since the point density does not support production of higher resolutions.

2.6. DEM assessment

To evaluate the vertical accuracy of the DEMs, 56 ground control points were measured with a Leica TCPR 1202 total station (accuracy ± 2 mm). Since the ground control points were a subset of the 62 pH soil sampling points, the requirement of random spatial distribution for reference data was fulfilled (c.f. section 2.3) (Höhle and Höhle, 2009). To assess vertical accuracy, the height differences Δh_i between the ground control points and the interpolated DEMs were calculated. Besides standard accuracy statistical measures (mean, standard deviation, absolute mean error, RMSE), robust measures were derived, which do not assume normally distributed errors and are more resistant to outliers (Höhle and Höhle, 2009). Since several studies have shown that a normal distribution of errors in DEMs derived from LiDAR data is not always given due to filtering and interpolation errors (Gallay et al., 2013; Höhle and Höhle, 2009; Zandbergen, 2011), we checked for deviations from normal distribution using quantile-quantile plots. In addition, the median, the normalized median absolute deviation (NMAD) and the 68.3% and 95% sample quantiles were used as robust measures. The NMAD, which is an estimate of standard deviation resilient to outliers in the error distribution (Höhle and Höhle, 2009), was calculated according to:

$$\mathrm{NMAD} = 1.4286 \bullet \mathrm{median}_j\left(\left|\Delta h_j - m_{\Delta h}\right|\right)$$

where Δh_j denotes the individual errors j = 1, …. n and $m_{\Delta h}$ is the median of the errors. Another approach used to deal with outliers is to remove them by applying a threshold, e.g. an error is classified as an outlier if $|\Delta h_j| > 3 \bullet$ RMSE. Standard accuracy measures were calculated before and after outlier removal.

2.7. Soil pH models

For all DEMs derived from TLS and ALS point clouds, for all resolutions (0.2, 0.5, 1, 2, 4 m) and for both interpolation methods, ordinary least squares (OLS) regression models were built. In addition, two DEMs based on the dataset SwissAlti were generated applying both interpolated methods for a cell size of 2 m. All statistical computations were done in R (v3.2.2, R Core Team).

2.7.1. Terrain attributes

For each DEM a set of Terrain Attributes (TAs) were calculated using the Python API of ArcGIS (v.10.3, ESRI) and SAGA GIS (v.2.1.2) (Table 2). This set of TAs comprised local TAs such as curvature or regional TAs such as TWI to represent hydrologically relevant properties of the terrain. As described in section 2.3, the relationship between topsoil pH and topography in a general sense is understood for the study area. Ridges, e.g. described by positive plan curvature values, show surface flow divergence and therefore tend to weathering which leads to low pH values. On the other hand, negative plan surfaces values describe depressions where convergence flow lines indicate an accumulation of basic cations in the soil water solution and therefore lead to a high pH. TWI indicates the amount of water flowing towards a certain location while the local slope, also integrated in the TWI formula, reflects subsurface lateral transmissivity. An overview how curvature and TWI affects soil properties are given in Shary and Pinskii (2013), McKenzie et al. (2000) and Wilson (2012). To derive the various terrain variables, we applied different computational methods which each likely produce slightly different results. Different equations and implementations to calculate curvature and TWI are given in Shary et al. (2002) and Hengl and Evans (2009) for curvature and in Wilson (2012) for TWI, respectively. Overall, 18 TAs were derived for each DEM, and through different parameter settings a total of 136 possible variables were calculated. For sake of readability, the different TAs including their derived variants using different computational methods are hereafter referred to as TAs.

To incorporate different spatial scales, the TAs were smoothed by local average filters. The filter was defined as a circle with distinct radii of 3, 6, 12 and 18 cells. TAs selected for the OLS pH models, their regression coefficients, the filter sizes and their significance regarding to soil formation are provided in the Supplementary Tables S1 and S2. A description of the applied implementations to derive the TAs is given in Supplementary Table S3.

Table 2
List of local and regional TAs derived from DEMs.

Terrain Attribute	Type	Reference
Slope steepness	Local	(Shary et al., 2002)
Plan curvature	Local	(Shary et al., 2002)
Profile curvature	Local	(Shary et al., 2002)
Mean curvature	Local	(Shary et al., 2002)
Minimal curvature	Local	(Shary et al., 2002)
Maximal curvature	Local	(Shary et al., 2002)
Tangential curvature	Local	(Krcho, 1991)
Cross-sectional curvature	Local	(Wood, 1996)
Longitudinal curvature	Local	(Wood, 1996)
Aspect (Eastness/Northness)	Local	(Shary et al., 2002)
Relative slope position	Regional	(MacMillan and Shary, 2009)
Topographic position index	Regional	(Weiss, 2001)
Melton Ruggedness Index	Regional	(Marchi and Dalla Fontana, 2005)
Flow path length	Regional	(Moore et al., 1991)
Topographic wetness index	Regional	(Wilson, 2012)
Upslope catchment height	Regional	(Wilson, 2012)
Stream power index	Regional	(Wilson, 2012)
Multiresolution index of valley bottom flatness	Regional	(Gallant and Dowling, 2003)

2.7.2. Model building

To reduce the large number of terrain variables (in this respect referred to as predictor variables), we first calculated a correlation matrix (Pearson r) for each DEM. If two predictor variables were highly correlated (Pearson's $r > |0.8|$) we retained the variable that was more strongly correlated with the pH target variable. We repeated this procedure until the correlations among all the predictor variables were lower |0.8|. The least absolute shrinking and selection operator (LASSO: Tibshirani, 1996) implemented in the GLMNET R package (v.2.0–2) was applied to exclude the likely non-relevant variables. LASSO is a method of penalized likelihood, which imposes a constraint on estimates of model parameters. Coefficients of variables which contribute least to the model, shrink to zero and are left out whereas variables with non-zero coefficients remain in the model (Hastie et al., 2009). A 10-fold-cross-validation determined the optimal LASSO penalty parameter λ. All variables with non-zero coefficients were selected from the most regularized model, for which the performance in terms of estimated expected generalization error is within one standard error of the minimum. For each pH model, the evolution of the mean square errors as function of the model complexity is shown in Supplementary Tables S1 and S2.

To obtain parsimonious OLS models with only significant terms, the selected variables were further reduced using Bayesian Information Criterion (BIC: Burnham and Anderson, 2004). We used quantile-quantile (Q-Q) plots, plots of residuals and Cook's distance plots to visually test whether the basic assumption of linear regressions were fulfilled and to check for outliers. Spatial autocorrelation of the residuals was calculated for each final model with Moran's I and correlograms over various lag distances (R package NCF v.1.1–5). P-values of Moran's I were corrected according to Holm. However, no significant spatial autocorrelation was detected in any of the models' residuals (Supplementary Tables S1 and S2).

2.7.3. Model evaluation

As a measure of the predictive power, we used the correlation of the predicted values with the observed values (R^2). We applied a 10-fold cross-validation. To test the random error associated with each 10-fold cross validation, the cross validation procedure was repeated 100 times. The final model performance (100 times 10-fold crossvalidated R^2) was based on the mean of 100 iterations of the cross-validation.

3. Results

3.1. Evaluation and comparison of the DEMs

Although the study site is characterized by a complex terrain with a dense evergreen forest canopy and a dense ground vegetation, the ALS and TLS ground point densities were high. The mean ground point density was 245.75 points/m^2 for the TLS, 6.69 points/m^2 for the ALS, but only 0.52 points/m^2 for the SwissAlti dataset. The 78 TLS scans led to a good coverage of the study area. 91% of all cells of a 1 m grid were covered by at least one TLS data point. The corresponding value was 81% for the ALS data whereas only 30% of the grid cells were covered by SwissAlti LiDAR points.

The Q-Q plots of the error distributions showed for all DEMs no or moderate departure from a normality (Supplementary Figures S1–S6). Errors in vertical height larger than 1 m were observed only for ALS and TLS with a resolution of 4 m, for both interpolation methods and for the SwissAlti DEMs. The median values revealed a systematic over prediction for all DEMs with the exception of TLS4m-TIN (Supplementary Table S4). The standard accuracy statistical measures were similar to their robust counterparts, which indicates that non-normality errors were not a serious

concern in this study. Therefore, the RMSE was used to discuss the accuracy of the DEMs since it is used in most studies. Generally, the higher the resolution, the more accurate were the DEMs as indicated by the RMSE of the various DEMs as a function of resolution (Fig. 2). The most accurate DEMs with RMSEs from 0.12 to 0.14 m were based on TLS data for resolutions between 0.2 and 0.5 m respectively, independent of the interpolation method. At a resolution of 1 m, the RMSE was nearly identical for the TLS and ALS DEMs. For cell sizes of 0.2, 0.5 and 1 m the TIN interpolator created slightly lower RMSE values compared to the IDW method. However, for larger cell sizes, ALS based DEMs interpolated with the TIN method were more accurate compared to the corresponding TLS elevation models, whereas this trend was not evident for the IDW interpolated DEMs. The RMSE values of the SwissAlti were considerably higher compared to the relevant TLS and ALS DEMs for both interpolation methods.

3.2. Soil pH models

The results of the OLS regression modelling revealed an overall scale dependency in the model prediction (Fig. 3. Supplementary Table S5). Generally, the model performance increased with increasing resolutions. However, the TIN based models with cell sizes of 0.2 m showed a lower R^2_{cv} compared to the models with 0.5 m resolutions (Fig. 3, A). TLS derived models with resolutions up to 1 m performed significantly better than the corresponding ALS models. The highest performance ($R^2_{cv} = 0.62$) was achieved for the TLS model with a cell size of 0.5 m generated by the TIN interpolation. The best ALS model ($R^2_{cv} = 0.5$) was obtained with the same resolution and interpolation method. ALS derived models with resolutions of 2 and 4 m generated with the TIN interpolation were better than the respective TLS models, whereas for the IDW interpolated models this trend could not be observed. The performance of OLS models based on the SwissAlti point cloud was considerably lower compared to the corresponding 2 m TLS and ALS models with a maximal R^2_{cv} of 0.21 (Fig. 3. Supplementary Table S5).

Most OLS models contained predictors describing curvature, flow path and topographic wetness indices. The higher the resolution, the more predictors were smoothed with a local average filter. OLS models based on cell sizes lager than 1 m contained no smoothed predictors anymore (Supplementary Tables S1 and S2).

The best OLS model (TLS0.5 m-TIN) was used to predict the topsoil pH for the entire study area (Fig. 4).

4. Discussion

The accuracy assessment of DEMs revealed, unsurprisingly, that the finer spatial resolution DEMs were generally more accurate than the coarser resolution surfaces, confirming previous studies (Bater and Coops, 2009; Saksena and Merwade, 2015; Liu, 2008).

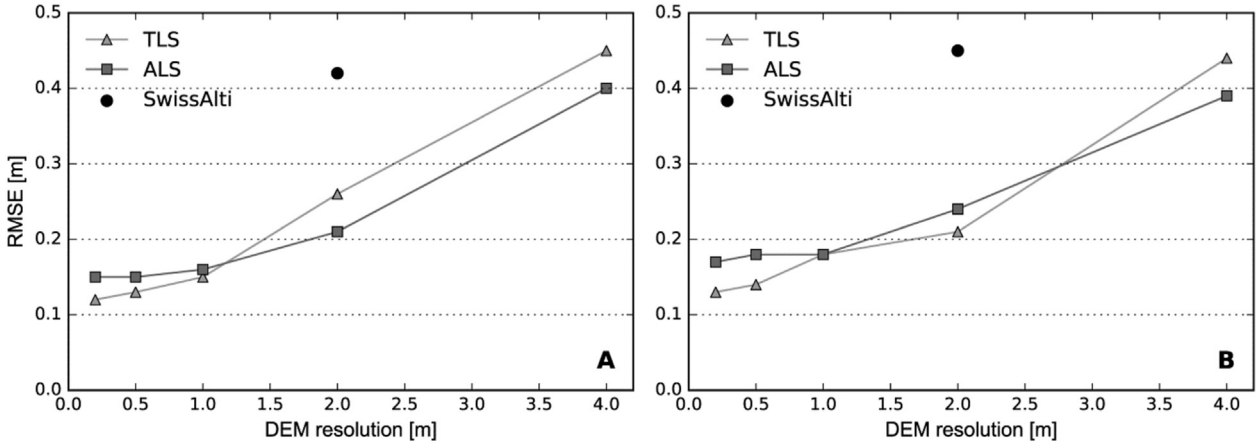

Fig. 2. Root mean square error (RMSE) for DEMs derived from ALS, TLS and SwissAlti data for different resolutions. A: Triangular irregular network (TIN) interpolation, B: Inverse distance weighting (IDW) interpolation.

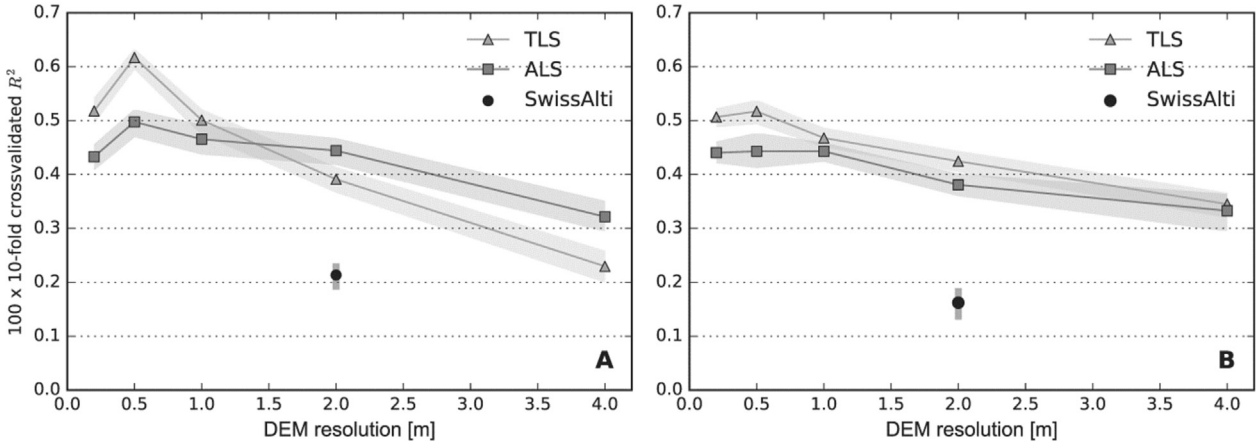

Fig. 3. Ordinary least squares (OLS) regression models results reported as 100 times 10 fold crossvalidated R^2 with 5% and 95% percentiles for different DEMs resolutions. A: Triangular irregular network (TIN) interpolation, B: Inverse distance weighting (IDW) interpolation.

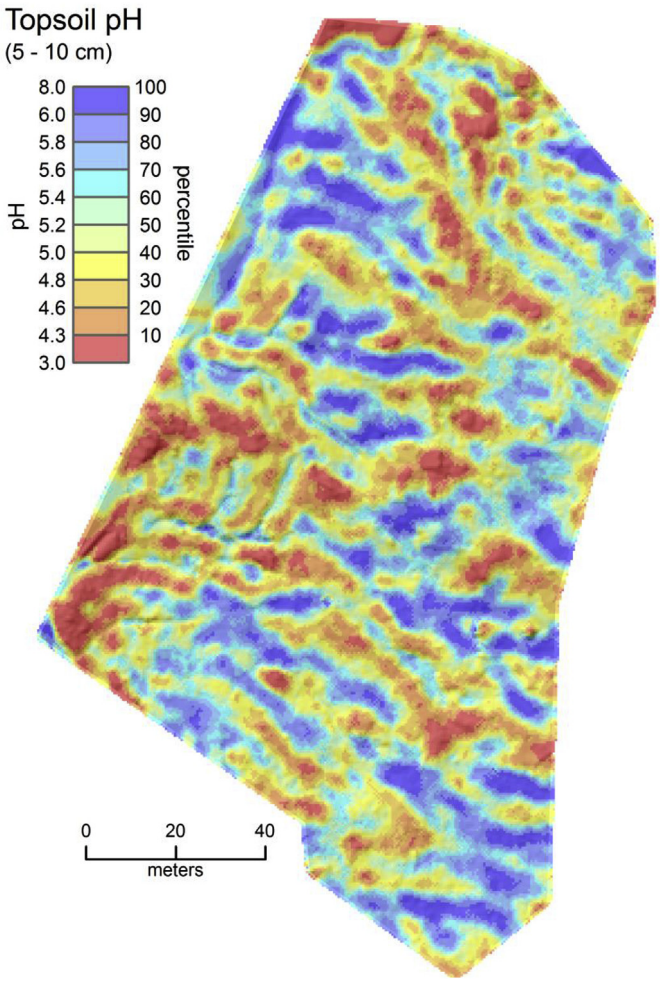

Fig. 4. Topsoil pH (5–10 cm depth) prediction based on the ordinary least squares (OLS) regression model TLS0.5 m-TIN.

Obviously, the micro-topography in the study area could not be described accurately with cell sizes larger than 1 m. The higher accuracy of the TLS based DEMs for resolutions of 0.2 and 0.5 m compared to the corresponding ALS elevation models shows that higher point densities improved the representation of the topography. This was the case in spite of the greatly variable TLS point distribution and the numerous individual TLS scans that had to be co-registered. The acquisition of TLS scans with different viewsheds helped to mitigate shadowing effects in the dense forest stand. Furthermore, the numerous scans led to a nearly complete coverage of the study area which is important for an evenly distributed quality of the DEMs.

The accuracy measures of the TLS-DEMs also revealed that the adaptive TIN filter, which was originally developed for ALS data (Axelsson, 2000), can be successfully used to separate the TLS point cloud into ground and non-ground points even in a complex environment. Several studies have argued that specific filter algorithm for TLS data need to be developed (Guarnieri et al., 2009; Panholzer and Prokop, 2013; Puttonen et al., 2015; Rodríguez-Caballero et al., 2016), but this was not the case in our study. Rather, we argue that accuracy is strongly influenced by the scan setup. The chance to identify appropriate TLS ground points is strongly dependent on scan distance ranges. If the scan distance increases, angle of incidence also increases due to the relatively low scanner height. Therefore, the number of possible ground points is reduced and the likelihood that the returned signal originates from non-ground objects increases (Puttonen et al., 2015). As a consequence, the heights of the identified ground points are overestimated with increasing distance from the scanner location. Therefore, the scan locations and the number of scans must be chosen appropriately, especially when larger areas are scanned. For distances greater than 15 m, Puttonen et al. (2015) identified the strongest increase of overestimation. Since the mean distance between the scan locations was 7.9 m in the present study, this overestimation was not a major issue. However, both TLS and ALS derived DEMs exhibited a systematic overestimation (e.g. median value for TLS0.2 m-TIN: −0.06 m, ALS0.2 m-TIN: −0.09 m). This finding is not surprising because the dense (ground) vegetation cover reduced the laser penetration to the ground, irrespective of the LiDAR acquisition technique.

Compared to other studies, the accuracies of both TLS and ALS derived DEMs is high, even in the complex environment studied here. For resolutions up to 0.5 m, we obtained RMSEs between 0.12 and 0.14 m for the TLS-DEMs (Fig. 2, Supplementary Table S4). For similar study regions and DEM resolutions Gallay et al. (2013) and Pirotti et al. (2013) reported RMSEs of 0.525 and 0.3 m, respectively. To acquire the TLS data, Gallay et al. (2013) used 7 scans to cover an area of 2.5 ha. The maximal scan distances in these two studies ranged from 100 to 350 m. The small scan distances used in our study most likely accounted for our higher accuracies. In addition, no point cloud filtering was applied by Gallay et al. (2013). However, separating ground from vegetation points is critical to derive DEMs in such complex environments. For the ALS DEMs, the high point density obtained by the low flight altitude and speed accounted for the high accuracy. The penetration rate (number of pulses that hit the ground as a percentage) was high (40%) considering the dense vegetation cover in the study area. The SwissAlti DEMs suffered from a low ground point density, an insufficient spatial coverage of the study area and a high vertical standard deviation.

Due to high sampling point density, small differences were observed between the employed interpolation techniques. The TIN interpolation provided slightly better results compared to the IDW method but no general suggestion can be drawn from this study concerning that aspect, and we argue that where point densities are sufficiently high choice of interpolator becomes less important. Guo et al. (2010) obtained similar results from investigations of different interpolation methods for dense LiDAR data.

In order to model topsoil pH adequately in the study area, TAs derived from very high resolution DEMs were required, because the pH varies over a large pH range within a distance of a few meters. The OLS models based on DEMs with 4 m resolutions were only about half as accurate as the best results. Our study emphasized the importance of using the appropriate scale even in sub-meter ranges, since the highest resolution (0.2 m) decreased the model accuracy again. Obviously, an optimal scale exists to model the relationship between terrain and pH of the soil. The reason for a decreased accuracy at 0.2 m resolutions may either be due to short-scale variations or “noise” which can be explained by real-world terrain variation or due to artifacts of DEM generation (Smith et al., 2006). Because the RMSE of the 0.2 m DEMs were lower or in one case equal to the corresponding 0.5 m DEMs, short scale-terrain variation, which does not influence topsoil pH, is likely to be the reason for the noise in our study.

Up to a resolution of 1 m, TLS based OLS models performed better than their ALS counterparts whereas for cell sizes larger than 1 m, ALS based models were similar or better (Fig. 3). This trend can be explained by the RMSE accuracy measures of the DEMs which paralleled these patterns (Fig. 2). Overall, the RMSEs describe the performance of the pH-models appropriately. However, the best OLS model, based on DEM TLS0.5 m-TIN, performed substantially

better than the others OLS models and better than expected based on RMSE values. Here, we have to consider that DEM accuracy measures represent point measures whereas the OLS models additionally rely on hydrologically relevant TAs that are dependent on upstream contributing areas. Small differences in slope values can propagate into significant variations in the calculated flow and can, in combination with the DEM resolution, strongly influence the model results (c.f. Hebeler and Purves, 2009).

The RMSEs of the Swisstopo DEMs indicated that the performance of the corresponding OLS models was low. Although the Swissalti DEM has been used in various studies for digital terrain modelling (e.g. Camathias et al., 2013; Nussbaum et al., 2014; Zellweger et al., 2013) it is not an adequate data source to describe small-scale topographic variation in forest stands.

The structure of the OLS models revealed that models based on resolutions from 0.2 to 1 m rely on smoothed predictors (Supplementary Tables S1 and S2). Too detailed terrain information may reduce the correlation between the predictor and the target variable. Local average filters applied e.g. on flow path predictors retain on the one hand the accurate flow path from high resolution DEMs, and on the other hand reduce the high-frequency variations.

5. Conclusions

Use of a TLS allowed us to create very high resolution and highly accurate DEMs in a complex environment with a strong microtopography and a dense vegetation cover. Our study revealed that accuracies were higher compared to DEMs derived from high quality helicopter based LiDAR data. This is also reflected in the performance of the pH models which were substantially better for TLS than the corresponding ALS models at high resolutions. Furthermore, the results showed that submeter DEM resolutions were required to accurately model topsoil pH in the present study area because the pH varied strongly within short distances. Since only TAs were used to create the pH models it can be concluded that the high point density provided by TLS improves the quality of topographical features extracted from DEMs in the submeter scale which is relevant for hydrological and ecological applications.

Although the co-registration of neighboring scans allowed us to create DEMs covering several hectares, TLS data acquisition is bound to substantial smaller areas as compared to ALS. The TLS field data acquisition took about 5 days and was the major cost factor whereas the TLS data processing was not a big issue since no manual editing was required.

The choice between TLS and ALS data acquisition is mainly given by the area under investigation. If highly accurate DEMs for complex study sites of a few hectares are required then TLS is the more favorable option over the well-established airborne LiDAR technique. LiDAR data obtained by unmanned aerial vehicles (UAV), might be a future alternative to acquire data over few hectares with an accuracy and ground point density coming close to the TLS data used in this study. Finally, there may be circumstances where fused models of ALS data (where penetration to ground is good) and TLS data (in more densely vegetated terrain) could be a feasible approach.

Software/data availability

The LiDAR software package LAStools is available from https://rapidlasso.com/lastools. The LAStools are freely available for all non-profit personal, non-military educational, or non-profit humanitarian purposes. Licensing is required for any commercial, government, or production use. The TLS and the helicopter based ALS point clouds are available as LAS files (378.5 and 11.5 MB) from https://drive.switch.ch/index.php/s/kd34pMRYSmH4ytV. The provided LAS-files contain unclassified and filtered ground points in the Swiss national coordinate system (CH1903LV03/LN02).

Acknowledgements

The authors thank Marco Walser and Roger Köchli for intensive field and labor work to handle the soil samples. We are grateful to Patrick Thee and Marielle Fraefel for the valuable help in the field survey. This work was partly funded by the SNSF in the frame of the national research program “Sustainable use of Soil as a Resource (NRP 68)”.

Appendix A. Supplementary data

Supplementary data related to this article can be found at http://dx.doi.org/10.1016/j.envsoft.2017.05.009.

References

Anderson, E.S., Thompson, J.A., Crouse, D.A., Austin, R.E., 2006. Horizontal resolution and data density effects on remotely sensed LIDAR-based DEM. Geoderma 132 (3–4), 406–415.
Arnone, E., Francipane, A., Scarbaci, A., Puglisi, C., Noto, L.V., 2016. Effect of raster resolution and polygon-conversion algorithm on landslide susceptibility mapping. Environ. Model. Softw. 84, 467–481.
Artuso, R., Bovet, S., Streilein, A., 2003. Practical methods for the verification of countrywide produced terrain and surface models. Int. Arch. Photogramm. Remote Sens. Spat. Inf. Sci. XXXXIV (3W/W13), 14–19.
Axelsson, P., 2000. DEM generation from laser scanner data using adaptive TIN models. Int. Arch. Photogramm. Remote Sens. 110–117. Amsterdam, The Netherlands.
Baltsavias, E.P., 1999. Airborne laser scanning: basic relations and formulas. ISPRS J. Photogrammetry Remote Sens. 54 (2–3), 199–214.
Bater, C.W., Coops, N.C., 2009. Evaluating error associated with lidar-derived DEM interpolation. Comput. Geosciences 35 (2), 289–300.
Behrens, T., Zhu, A.X., Schmidt, K., Scholten, T., 2010. Multi-scale digital terrain analysis and feature selection for digital soil mapping. Geoderma 155 (3–4), 175–185.
Bühler, Y., Marty, M., Egli, L., Veitinger, J., Jonas, T., Thee, P., Ginzler, C., 2015. Snow depth mapping in high-alpine catchments using digital photogrammetry. Cryosphere 9 (1), 229–243.
Burnham, K.P., Anderson, D.R., 2004. Multimodel inference: understanding AIC and BIC in model selection. Sociol. Methods & Res. 33 (2), 261–304.
Camathias, L., Bergamini, A., Küchler, M., Stofer, S., Baltensweiler, A., 2013. High-resolution remote sensing data improves models of species richness. Appl. Veg. Sci. 539–551.
Cavazzi, S., Corstanje, R., Mayr, T., Hannam, J., Fealy, R., 2013. Are fine resolution digital elevation models always the best choice in digital soil mapping? Geoderma 195–196 (0), 111–121.
Chaplot, V., Darboux, F., Bourennane, H., Leguédois, S., Silvera, N., Phachomphon, K., 2006. Accuracy of interpolation techniques for the derivation of digital elevation models in relation to landform types and data density. Geomorphology 77 (1–2), 126–141.
Chu, H.-J., Wang, C.-K., Huang, M.-L., Lee, C.-C., Liu, C.-Y., Lin, C.-C., 2014. Effect of point density and interpolation of LiDAR-derived high-resolution DEMs on landscape scarp identification. GIScience Remote Sens. 51 (6), 731–747.
Danson, F.M., Hetherington, D., Morsdorf, F., Koetz, B., Allgöwer, B., 2006. Three-dimensional forest canopy structure from terrestrial laser scanning. In: Koukal, T., Schneider, W. (Eds.), 3D Remote Sensing in Forestry, pp. 61–65. Vienna.
Dassot, M., Constant, T., Fournier, M., 2011. The use of terrestrial LiDAR technology in forest science: application fields, benefits and challenges. Ann. For. Sci. 68 (5), 959–974.
Fisher, P., Wood, J., Cheng, T., 2004. Where is Helvellyn? Fuzziness of multi-scale landscape morphometry. Trans. Inst. Br. Geogr. 29 (1), 106–128.
Gallant, J.C., Dowling, T.I., 2003. A multiresolution index of valley bottom flatness for mapping depositional areas. Water Resour. Res. 39 (12) (n/a-n/a).
Gallay, M., Lloyd, C.D., McKinley, J., Barry, L., 2013. Assessing modern ground survey methods and airborne laser scanning for digital terrain modelling: a case study from the Lake District, England. Comput. Geosciences 51, 216–227.
Grinand, C., Arrouays, D., Laroche, B., Martin, M.P., 2008. Extrapolating regional soil landscapes from an existing soil map: sampling intensity, validation procedures, and integration of spatial context. Geoderma 143 (1–2), 180–190.
Guan, H., Li, J., Yu, Y., Zhong, L., Ji, Z., 2014. DEM generation from lidar data in wooded mountain areas by cross-section-plane analysis. Int. J. Remote Sens. 35 (3), 927–948.
Guarnieri, A., Vettore, A., Pirotti, F., Menenti, M., Marani, M., 2009. Retrieval of small-relief marsh morphology from Terrestrial Laser Scanner, optimal spatial filtering, and laser return intensity. Geomorphology 113 (1–2), 12–20.

Guisan, A., Zimmermann, N.E., 2000. Predictive habitat distribution models in ecology. Ecol. Model. 135 (2–3), 147–186.
Guo, Q.H., Li, W.K., Yu, H., Alvarez, O., 2010. Effects of topographic variability and lidar sampling density on several DEM interpolation methods. Photogrammetric Eng. Remote Sens. 76 (6), 701–712.
Gurtz, J., Baltensweiler, A., Lang, H., 1999. Spatially distributed hydrotope-based modelling of evapotranspiration and runoff in mountainous basins. Hydrol. Process. 13 (17), 2751–2768.
Hastie, T., Tibshirani, R., Friedman, J., 2009. The Elements of Statistical Learning: Data Mining, Inference and Prediction, 2 nd ed. Springer, New York.
Hebeler, F., Purves, R.S., 2009. The influence of elevation uncertainty on derivation of topographic indices. Geomorphology 111 (1–2), 4–16.
Hengl, T., 2006. Finding the right pixel size. Comput. Geosciences 32 (9), 1283–1298.
Hengl, T., Evans, I.S., 2009. Chapter 2 mathematical and digital models of the land surface. In: Tomislav, H., Hannes, I.R. (Eds.), Developments in Soil Science. Elsevier, pp. 31–63.
Heritage, G., Hetherington, D., 2007. Towards a protocol for laser scanning in fluvial geomorphology. Earth Surf. Process. Landforms 32 (1), 66–74.
Heritage, G.L., Milan, D.J., Large, A.R.G., Fuller, I.C., 2009. Influence of survey strategy and interpolation model on DEM quality. Geomorphology 112 (3–4), 334–344.
Hilker, T., van Leeuwen, M., Coops, N., Wulder, M., Newnham, G., Jupp, D.B., Culvenor, D., 2010. Comparing canopy metrics derived from terrestrial and airborne laser scanning in a Douglas-fir dominated forest stand. Trees 24 (5), 819–832.
Hodgson, M.E., Jensen, J.R., Schmidt, L., Schill, S., Davis, B., 2003. An evaluation of LIDAR- and IFSAR-derived digital elevation models in leaf-on conditions with USGS Level 1 and Level 2 DEMs. Remote Sens. Environ. 84 (2), 295–308.
Höhle, J., Höhle, M., 2009. Accuracy assessment of digital elevation models by means of robust statistical methods. ISPRS J. Photogrammetry Remote Sens. 64 (4), 398–406.
Hyyppä, J., Hyyppä, H., Leckie, D., Gougeon, F., Yu, X., Maltamo, M., 2008. Review of methods of small-footprint airborne laser scanning for extracting forest inventory data in boreal forests. Int. J. Remote Sens. 29 (5), 1339–1366.
Isenburg, M., 2015. LAStools – Efficient Tools for LiDAR Processing, Version 150605.
Jakubowski, M.K., Guo, Q., Kelly, M., 2013. Tradeoffs between lidar pulse density and forest measurement accuracy. Remote Sens. Environ. 130 (0), 245–253.
Kim, D., Zheng, Y., 2011. Scale-dependent predictability of DEM-based landform attributes for soil spatial variability in a coastal dune system. Geoderma 164 (3–4), 181–194.
Kim, D., Cairns, D.M., Bartholdy, J., Morgan, C.L.S., 2011. Scale-dependent correspondence of floristic and edaphic gradients across salt marsh creeks. Ann. Assoc. Am. Geogr. 102 (2), 276–294.
Kobler, A., Pfeifer, N., Ogrinc, P., Todorovski, L., Oštir, K., Džeroski, S., 2007. Repetitive interpolation: a robust algorithm for DTM generation from Aerial Laser Scanner Data in forested terrain. Remote Sens. Environ. 108 (1), 9–23.
Krcho, J., 1991. Georelief as a subsystem of landscape and the influence of morphometric parameters of georelief on spatial differentiation of landscape-ecological processes. Ecol. (CSFR) 10, 115–157.
Lei, F., Atkinson, P.M., 2015. Accuracy of digital elevation models derived from terrestrial laser scanning data. Geoscience Remote Sens. Lett. IEEE 12 (9), 1923–1927.
Lin, Z., Kaneda, H., Mukoyama, S., Asada, N., Chiba, T., 2013. Detection of subtle tectonic–geomorphic features in densely forested mountains by very high-resolution airborne LiDAR survey. Geomorphology 182 (0), 104–115.
Liu, Xiaoye, 2008. Airborne LiDAR for DEM generation: some critical issues. Prog. Phys. Geogr. 32 (1), 31–49.
Liu, J.G., Mason, P.J., Liu, J.G., Mason, P.J., 2009. Filtering and Neighbourhood Processing, Essential Image Processing and GIS for Remote Sensing. John Wiley & Sons, Inc, pp. 37–55.
MacMillan, R.A., Shary, P.A., 2009. Chapter 9 Landforms and Landform Elements in Geomorphometry, 33, pp. 227–254.
Maguya, A., Junttila, V., Kauranne, T., 2014. Algorithm for extracting digital terrain models under forest canopy from airborne LiDAR data. Remote Sens. 6 (7), 6524–6548.
Marchi, L., Dalla Fontana, G., 2005. GIS morphometric indicators for the analysis of sediment dynamics in mountain basins. Environ. Geol. 48 (2), 218–228.
Marselis, S.M., Yebra, M., Jovanovic, T., van Dijk, A.I.J.M., 2016. Deriving comprehensive forest structure information from mobile laser scanning observations using automated point cloud classification. Environ. Model. Softw. 82, 142–151.
Maynard, J.J., Johnson, M.G., 2014. Scale-dependency of LiDAR derived terrain attributes in quantitative soil-landscape modeling: effects of grid resolution vs. neighborhood extent. Geoderma 230–231 (0), 29–40.
McBratney, A.B., Mendonça Santos, M.L., Minasny, B., 2003. On digital soil mapping. Geoderma 117 (1–2), 3–52.
McKenzie, N.J., Gessler, P.E., Ryan, P.J., O'Connell, D.A., 2000. The role of terrain analysis in soilmapping. In: Gallant, J.C., Wilson, J.P. (Eds.), Terrain Analysis: Principles and Applications. Wiley, New York, pp. 245–265.
Montealegre, A., Lamelas, M., Riva, J., 2015. Interpolation routines assessment in ALS-derived digital elevation models for forestry applications. Remote Sens. 7 (7), 8631–8654.
Moore, I.D., Grayson, R.B., Ladson, A.R., 1991. Digital terrain modelling: a review of hydrological, geomorphological, and biological applications. Hydrol. Process. 5 (1), 3–30.
Moskal, L.M., Zheng, G., 2011. Retrieving forest inventory variables with terrestrial laser scanning (TLS) in urban heterogeneous forest. Remote Sens. 4 (12), 1–20.
Mulder, V.L., de Bruin, S., Schaepman, M.E., Mayr, T.R., 2011. The use of remote sensing in soil and terrain mapping — a review. Geoderma 162 (1–2), 1–19.
Nussbaum, M., Papritz, A., Baltensweiler, A., Walthert, L., 2014. Estimating soil organic carbon stocks of Swiss forest soils by robust external-drift kriging. Geosci. Model Dev. 7 (3), 1197–1210.
Pain, C.F., 2005. Size does matter: relationships between image pixel size and landscape process scales, MODSIM, 2005. International Congress of Modelling and Simulation. Modelling and Simulation Society of Australia and New Zealand Inc. Citeseer, pp. 1430–1436.
Panholzer, H., Prokop, A., 2013. Wedge-filtering of geomorphologic terrestrial laser scan data. Sensors 13 (2), 2579–2594.
Park, S., Ruecker, G., Agyare, W., Akramhanov, A., Kim, D., Vlek, P., 2009. Influence of grid cell size and flow routing algorithm on soil–landform modeling. J. Korean Geogr. Soc. 44 (2), 122–145.
Pirotti, F., Guarnieri, A., Vettore, A., 2013. Ground filtering and vegetation mapping using multi-return terrestrial laser scanning. ISPRS J. Photogrammetry Remote Sens. 76 (0), 56–63.
Puttonen, E., Krooks, A., Kaartinen, H., Kaasalainen, S., 2015. Ground level determination in forested environment with utilization of a scanner-centered terrestrial laser scanning configuration. Geoscience Remote Sens. Lett. IEEE 12 (3), 616–620.
Rodríguez-Caballero, E., Afana, A., Chamizo, S., Solé-Benet, A., Canton, Y., 2016. A new adaptive method to filter terrestrial laser scanner point clouds using morphological filters and spectral information to conserve surface microtopography. ISPRS J. Photogrammetry Remote Sens. 117, 141–148.
Rossiter, D.G., 2005. Towards a Multiple-use Soil Information System.
Sačkov, I., Kardoš, M., 2014. Forest delineation Based on LiDAR Data and Vertical Accuracy of the Terrain Model in Forest and Non-forest Area.
Saksena, S., Merwade, V., 2015. Incorporating the effect of DEM resolution and accuracy for improved flood inundation mapping. J. Hydrology 530, 180–194.
Samuel-Rosa, A., Heuvelink, G.B.M., Vasques, G.M., Anjos, L.H.C., 2015. Do more detailed environmental covariates deliver more accurate soil maps? Geoderma 243–244, 214–227.
Schaub, M., Dobbertin, M., Kräuchi, N., Kaennel Dobbertin, M., 2011. Preface-long-term ecosystem research: understanding the present to shape the future. Environ. Monit. Assess. 174 (1), 2.
Schleppi, P., Muller, N., Feyen, H., Papritz, A., Bucher, J.B., Flühler, H., 1998. Nitrogen budgets of two small experimental forested catchments at Alptal, Switzerland. For. Ecol. Manag. 101 (1–3), 177–185.
Seibert, J., Stendahl, J., Sørensen, R., 2007. Topographical influences on soil properties in boreal forests. Geoderma 141 (1–2), 139–148.
Shary, P.A., Pinskii, D.L., 2013. Statistical evaluation of the relationships between spatial variability in the organic carbon content in gray forest soils, soil density, concentrations of heavy metals, and topography. Eurasian Soil Sci. 46 (11), 1076–1087.
Shary, P.A., Sharaya, L.S., Mitusov, A.V., 2002. Fundamental quantitative methods of land surface analysis. Geoderma 107 (1–2), 1–32.
Smith, M.P., Zhu, A.X., Burt, J.E., Stiles, C., 2006. The effects of DEM resolution and neighborhood size on digital soil survey. Geoderma 137 (1–2), 58–69.
Swisstopo, 2010. Height models. In: Swisstopo, S.F.O.o.T. (Ed.), Swiss Federal Office of Topography Swisstopo. Wabern.
Tarolli, P., 2014. High-resolution topography for understanding Earth surface processes: opportunities and challenges. Geomorphology 216 (0), 295–312.
Tibshirani, R., 1996. Regression shrinkage and selection via the lasso. J. R. Stat. Soc. Ser. B 58 (1).
Walthert, L., Graf Pannatier, E., Meier, E.S., 2013. Shortage of nutrients and excess of toxic elements in soils limit the distribution of soil-sensitive tree species in temperate forests. For. Ecol. Manag. 297, 94–107.
Wang, G., Joyce, J., Phillips, D., Shrestha, R., Carter, W., 2013. Delineating and defining the boundaries of an active landslide in the rainforest of Puerto Rico using a combination of airborne and terrestrial LIDAR data. Landslides 10 (4), 503–513.
Weiss, A.D., 2001. Topographic position and landforms analysis. In: ESRI (Ed.), ESRI User Conference (San Diego CA).
Wilson, J.P., 2012. Digital terrain modeling. Geomorphology 137 (1), 107–121.
Wood, J.D., 1996. The Geomorphological Characterisation of Digital Elevation Models. University of Leicester, UK.
Yang, P., Ames, D.P., Fonseca, A., Anderson, D., Shrestha, R., Glenn, N.F., Cao, Y., 2014. What is the effect of LiDAR-derived DEM resolution on large-scale watershed model results? Environ. Model. Softw. 58, 48–57.
Zandbergen, P.A., 2011. Characterizing the error distribution of lidar elevation data for North Carolina. Int. J. Remote Sens. 32 (2), 409–430.
Zellweger, F., Braunisch, V., Baltensweiler, A., Bollmann, K., 2013. Remotely sensed forest structural complexity predicts multi species occurrence at the landscape scale. For. Ecol. Manag. 307 (0), 303–312.